LAWRENCE
LIVERMORE
NATIONAL
LABORATORY

UCRL-JRNL-221336

Zinc Single Crystal Deformation Experiments using a "6 Degrees of Freedom" Apparatus

D. H. Lassila, M. M. LeBlanc, J. N. Florando

May 12, 2006

Metallurgical and Materials Transactions A

Disclaimer

Zinc Single Crystal Deformation Experiments using a "6 Degrees of Freedom" Apparatus

D. H. Lassila, M. M. LeBlanc, and J. N. Florando

Abstract

A new experimental technique to study crystallographic slip system activity in metallic single crystals deformed under a condition of uniaxial stress is applied to study the behavior of Zn single crystals. The experimental apparatus allows essentially unconstrained shape change of inherently anisotropic materials under a condition of uniaxial stress by allowing 3 translational and 3 rotational degrees of freedom during compression; hence we have named the experiment 6 degrees of freedom (6DOF). The experiments also utilize a 3-D digital image correlation system to measure full-field displacement fields, which are used to calculate strain and make direct observations of slip system activity. We show that the experimental results associated with a pristine zinc single crystal are precisely consistent with the theoretical predicted shape change (sample distortion) assuming that the most favored slip system on the basal plane is the only one that is active. Another experiment was performed on a processed and annealed Zn single crystal to investigate slip that is inconsistent with the critical resolved shear stress (CRSS) theory. These experiments on zinc illustrate the ability of the 6DOF experiment, together with image correlation (IC) data, to measure slip system activity with a high degree of fidelity.

KEY WORDS- Single crystal, compression test, plasticity, resolved shear stress

I. Introduction

The mechanical behavior of metallic single crystals has been a subject of great interest since the discovery and quantification of the crystal lattice using X-ray diffraction techniques. The first plasticity studies performed mainly focused on the relationships between plastic flow and crystallographic "slip planes" and "slip directions"; for example

the work of Taylor and Elam in the late 1920s identified the <111> slip directions and (110) slip planes in fcc metals.[1, 2] The seminal work of Schmid and co-workers in the 1930s led to the development of what is referred to as the "critical resolved shear stress law" that states slip takes place along a given plane and direction when the resolved shear stress acting along them reaches a critical value.[3] While the initial work in this field was pivotal, it was also incomplete in many regards and lacked, in general, a comprehensive approach due to the limitations of the available experimental techniques and diagnostics of the day. For example, some early studies to identify active slip systems focused only on slip trace analyses, without fully accounting for the effects from the crystal loading and experimental boundary conditions.[4]

From a mechanics standpoint, the inherent difficulty in single crystal deformation experiments is the anisotropic nature of plastic flow when a single slip system dominates. For example, when a crystal is extended, the dominant slip system will cause the test sample to shear sideways as illustrated in Figure 1a.[5] However, in a tensile experiment the sample is constrained by the grips and as a result, lattice rotation and non-axisymmetric distortion of the sample occurs (Figure 1b). Clearly, bending and non-axisymmetric loads will cause inhomogeneities in the stress state throughout the test sample, leading to uncertainties in the resolved shear stresses driving the plastic deformation and effects on slip system activity.

Like tension experiments, compression experiments on single crystals such as those performed by Taylor and co-workers,[6] also have significant boundary condition issues that remain unresolved. In these experiments "single slip" will cause lattice rotation relative to the compression axis as shown in Figure 1c. The friction in these experiments can cause variations in the slip system driving stress in the test sample. While efforts are always employed to minimize friction using various techniques, e.g., periodic lubrication, Teflon film, etc., the friction and kinematics constraints of the platens on slip-system activity is problematic. Typically the stress state is assumed to be uniaxial and uniform if the deformation of the compression sample is approximately "uniform." However, this may not be the case since a wide range of combinations of slip system activity could result in a given shape change.

In this work, we have applied a new experimental technique to a very old problem; the deformation response of zinc single crystals. The experimental technique allows essentially unconstrained shape change of single crystals under a condition of uniaxial compression loading with a negligible friction boundary condition. We first describe the "6 Degrees of Freedom" (6DOF) experimental apparatus and the application of an image correlation (IC) technique to measure shape change and surface displacements. The effect of slip activity on distortion of a zinc crystal and resulting variation in the uniaxial stress state is determined . While the result presented on high-quality as-grown zinc single crystal is shown to be consistent with the critical resolved shear stress (CRSS) theory, other results on a processed and annealed zinc single crystal are not consistent.

II. Description of the 6DOF Experiment

The objective of the 6DOF compression experiment is to allow, as best as possible, unconstrained shape change in a test sample while maintaining a uniaxial stress state. As illustrated in Figure 2, the upper platen is a half sphere, allowing tilt in two directions and axial displacement, and the bottom platen is mounted on a ball bearing surface, allowing translation in two directions and twist about the compression axis, totaling six degrees of freedom. A detailed finite element analysis of the experiment was performed to assess the tolerances needed so that the axial stress was within 2% of the nominal value. It was determined that the most critical issue was alignment of the axis of the half sphere over the center of the test sample. To facilitate a precise alignment, a series of fixtures were designed and built with tight dimensional tolerances with respect to alignment, as shown and further described in Figure 3. We point out here that as the bottom of the test sample translates with respect to the top during the test, a non-uniform stress state will develop due to a bending moment. This non-uniform stress state, which is analyzed using finite element analysis in section IV, essentially puts a limit on the deformation that can be accommodated by the apparatus.

The lower platen of the 6DOF apparatus rests on a surface covered with 500 μm diameter tungsten carbide balls so that as the crystal bottom translates and/rotates during

deformation, it encounters a minimal constraint. Some consideration was given to the diameter of the balls because the rolling friction is proportional to the inverse of the diameter.[7] However, the experiment was designed to be performed up to relatively high strain rates (1.0 s^{-1}) for the purpose of validation of 3-D crystal plasticity simulations and at high rates, rotational inertia could also be a considerable drag force preventing free shape change of the test sample. The 500 μm ball diameter was chosen based on an estimate of these competing effects. The rolling friction was measured experimentally as a function of axial load and was found to be 0.02 (ratio of the force required for translation to axial load). An experiment was also performed to evaluate the friction typically encountered for a copper test sample translating on a lubricated and polished tungsten carbide platen. This data, shown in Table I, suggests that the ball bearing platen results in a substantial reduction of friction coefficient by a factor of 6 or more. Most importantly, the rolling friction was found to increase gradually to its maximum value, where as the metal-on-metal situation first encounters static friction from which the sample must break free.

Table I.

	Translation Platen	Lubricated metal against carbide
Kinetic friction coefficient	0.02	0.12
Static friction coefficient	—	0.14

The zinc test samples were glued with an epoxy to the platens (top and bottom) in the experiments reported in this paper so that the test sample stayed in good alignment with the apparatus. In these experiments a zone of material adjacent to the platen by in large did not deform plastically (as will be shown in the next section), and because of this the glue joint probably had little or no effect on the experimental results. We note here that the elastic Poisson effect (i.e. lateral expansion) is very small because of the very low yield strength of the zinc single crystals. We also note that the corners of the specimens in contact with the platens are elastic stress concentrations and could promote the initiation of slip. While the analysis of the samples in this study do not appear to show initiation of slip from the corners, future experiments and analysis on samples with a

reduced gage section will be conducted to minimize the effect of the platen-sample stress concentration.

The 6DOF experiment was originally designed to utilize a comprehensive variety of diagnostics to measure the shape change, local strains, translations, tilt, and rotations of the test sample during deformation. For example, in a previous publication, we reported the results of a series of experiments performed on molybdenum samples with resistance strain-gage rosettes used to measure strains during deformation.[8] Also, laser displacement gages have been used to measure translation/rotation of the lower platen, and extensometers have been used to measure the tilt and axial displacement of the half sphere relative to the lower platen. In this work, we have employed the IC technique to measure surface strains on the test sample and motion of the translation platen. A series of experiments were performed to compare and contrast IC and strain gage techniques which showed that the IC data is consistent with the more accurate, but local, strain gage measurements.[9]

III. Experimental Results

The slip behavior of hexagonal close pack (HCP) metals and alloys has been studied extensively, and it has been widely reported that in the case of Zn the (0001) basal slip plane and the three close pack <1112> directions are the slip systems with the lowest value of CRSS relative to other non-basal glide posibilities.[10-12] This behavior makes Zn a logical choice as a test material to benchmark the performance of the 6DOF experiment.

High purity [0001] zinc single crystals were grown using the Bridgman technique by Accumet Inc., Briarcliff Manor, New York. The nominal purity was found to be 99.98% and the list of impurities detected is given in Table II. A test sample was fabricated by careful mechanical polishing using silicon carbide paper. Inspection of the test sample prior to testing indicated that the top and bottom surfaces were parallel to within $\pm$12 μm. The crystallographic orientation with respect to the laboratory coordinate system is shown in Figure 4, along with a stereographic projection, which shows the most favored slip direction on the basal slip plane.

Table II. Zinc single crystal chemical analysis (as-grown) in ppmw.

C	O	Na	Si	Cl	Ca	Fe	Ni	Cu	Mo	Sb
14	5	0.085	0.079	0.16	0.055	0.20	0.068	0.24	0.023	0.033

The test sample and 6DOF fixtures were assembled as shown in Figure 3. An extensometer was used to measure the displacement of the half sphere relative to the bottom platen, and a 300 lb. load cell was used to measure the axial load during compression. The experiment was performed in a 50,000 lb. capacity screw driven test machine. While the 6DOF apparatus was designed to allow testing at relatively high strain rates, the experiments reported here were performed at a quasi-static strain rate of 10^{-4} s^{-1} (axial displacement rate of 1.4 x 10^{-6} m/s) to allow better utilization of the IC technique. The axial stress-strain response determined from the load cell and extensometer data is shown in Figure 5.

The IC technique is a powerful and versatile diagnostic to determine the global shape change of the test sample, axial strain, and as will be shown, direct measurement of the shear strain of the primary slip system. During the compression of the Zn crystal, IC was used to measure the full-field displacement fields of two adjacent sides of the test sample (A and B shown in Figure 4) at a rate of 1 image per second and a shutter speed of 15 ms. The other two sides of the sample (C and D) were analyzed based on static shots of the surfaces before and after deformation. The details of the image correlation technique to determine displacement fields and calculation of surface strains are given elsewhere.[13, 14] In Figure 6, the axial strains as they developed during deformation are shown. From this data, the axial strain during deformation was determined based on the effective (or active) gage length of the test sample, G_{eff}, which accounts for the angle, α that the primary slip plane makes with the compression axis and is given by the following equation:

$$G_{eff} = L - \frac{W}{Tan(\alpha)} = 15.5 - \frac{5.575}{Tan(72.4°)} = 13.73mm \qquad (1)$$

where L and W are the length and width of the test sample respectively. We note here that the sample deformation was nearly plane strain based on the observation that sides A

and C of the test sample did not change shape, which is consistent with only the primary system being active. Also inhomogeneous bands of deformation can be seen on sides B and D that are parallel with the basal plane suggesting glide on the primary system.

The IC data was used to determine the actual motion of the translation platen relative to the top of the test sample, and this motion was found to be precisely consistent with the primary slip system being the only active slip system. The theoretical translation of the test sample assuming single slip occurs over the effective gage length (equation 1) is given by the following formula:

$$T_x = -\varepsilon_f * G_{eff} * \mathrm{Tan}(\theta_1) * \mathrm{Cos}(\theta_2) \qquad (2a)$$

$$T_y = -\varepsilon_f * G_{eff} * \mathrm{Tan}(\theta_1) * \mathrm{Cos}(\theta_3) \qquad (2b)$$

where ε_f is the final axial strain, θ_1 is the angle that the slip plane makes with the compression axis, θ_2 is the angle the slip direction makes with projection of the x-axis on the slip plane, and θ_3 is the angle the slip direction makes with projection of the y-axis on the slip plane, as shown in Figure 7a. This analysis assumes no lattice rotation occurs during the deformation, which is a unique condition for the 6DOF experiment as illustrated in Figure 1. In Figure 7b, the experimentally observed translation based on IC measurements is shown to be in excellent agreement with the theoretical translation assuming slip activity only on the primary slip system, where θ_1= 72.4°, θ_2= 172°, and θ_3= 98°.

IV. Analysis of Stress States and Slip System Hardening

The 6DOF experiment was designed to apply a uniform uniaxial compressive stress state to a single crystal test sample, and the initial loading is essentially perfect in this regard due to the precision of the 6DOF fixtures and test sample geometry. However, as the sample distorts during deformation as described above and shown in Figure 7b, the axial loading will become increasingly non-uniform leading to a bending moment and non-uniform stress states. Hence, one of the critical issues is the variation of axial stress

(and resolved shear stresses of slip systems) associated with this phenomenon. To determine the maximum degree of non-uniformity, a linear elastic finite element analysis was performed using the final distorted geometry of the test sample, as shown in Figure 8. This analysis suggests that the maximum variation in axial stress was $\pm$10% at a nominal compression strain of 0.6%, which we believe to be acceptable for the purposes of establishing structure-property relationships for metallic single crystals. The axial stress-strain curve showing the calculated variation in axial stress is shown along with the axial stress-strain response determined using the load cell/extensometer data in Figure 5.

The primary slip-plane normal and slip direction are very close to being in the x-z plane of the laboratory coordinate system, as shown in Figure 4. Therefore, it is possible to directly observe the shear strain on the primary system in the x-z plane using the image correlation technique, with only a slight error introduced due to these misalignments with the side of the sample. In Figure 9, the image correlation data is shown with respect to an x'-z' coordinate system that is closely aligned with the primary slip plane. The gradient in displacement, du_x'/dz', is a direct observation of the primary slip system, assuming that no other slip systems are active.

A plot of the resolved shear-stress versus shear-strain for the primary slip system was constructed using the IC data and the load cell data (Figure 10). The work hardening rate calculated from the data is 1.4×10^{-4}G, where G is the shear modulus of the crystal. This result is consistent with hardening values for stage I "easy glide" regimes in other single crystal tests.[15] The variation in resolved shear stress on the tau-gamma plot were determined from the FEM analysis. It should be pointed out that the work hardening rate calculated from the tau-gamma curve could be substantially different depending on how the IC data is averaged. This is due to inhomogeneities in the deformation response of the zinc that is most clearly shown in the IC data presented in Figure 6. For example, in a very local region the accumulated strain on the primary slip system is only 20% of the average value given in Figure 6. The reasons for these relatively large extents of non-uniform behavior are not known, but are perhaps related to segregation of impurities during the crystal production.

V. Discussion

In previous experimental works on the deformation response of metallic single crystals, little attention has been given to boundary conditions that potentially can have a significant effect on slip system activity. While many references have reported results which are inconsistent with the critical resolved shear stress theory, the results were, in general, considered to be anomalous and possibly due to unknown effects of various boundary conditions, such as bending moments and frictional forces.

In this paper, we describe the 6DOF experiment and the results of an experiment performed on a zinc single crystal oriented for single slip on the basal plane. In this experiment, the boundary conditions were carefully controlled and only a small frictional force due to rolling of the translation platen prevented free glide of crystallographic slip systems, which in zinc are listed in Table III. Also shown in Table III, the critical resolved shear stress for slip along $<11\bar{2}0>$ slip directions on the basal plane is more than a factor of 10 less than slip that can occur on prismatic and pyramidal planes, and is thus highly favored. Although the Schmid Factor for some slip systems on the pyramidal planes are higher than for the basal plane, the maximum resolved shear stress never reaches the critical value to initiate slip on those systems. In addition, the translation of the sample during the compression experiment (Figure 7) is consistent with slip occurring only in the basal plane. Thus, the 6DOF experiments allow a careful and well-understood means of measuring the slip system response of metallic single crystals.

Table III. Critical resolved shear stresses and Schmid Factors for the three most common slip systems families in zinc.[16]

Plane/direction	CRSS (MPa)	Schmid Factor for $[22\ \bar{3}\bar{2}\ 10\ \bar{7}\bar{5}]$ sample	Schmid Factor for $[\bar{2}4\bar{2}3]$ sample
Basal $\{0001\}\ <11\bar{2}0>$	0.4	0.31	0.50
Pyramidal[17] $\{11\bar{2}\bar{2}\}<\bar{1}\bar{1}23>$	4-10	0.17 - 0.50	0.0 - 0.30
Prismatic[18] $\{1\bar{1}00\}\ <11\bar{2}0>$	6-15	0.02 - 0.05	0.0 - 0.23

While perfect zinc single crystals exhibit response consistent with the critical resolved shear stress theory, examples of non-basal glide and so-called “non-Schmid”

effects have been reported for other hcp metals. For example, in the work of Mark, Polanyi and Schmid[11] on thin zinc wires, slip trace observations were reported that suggested substantial amounts of slip accompanying the slip activity on the primary system. Brown[4] reported "cross slip" that was normal to the basal plane in cadmium (Cd), another hcp metal which has very similar slip response to zinc because of a similar c/a ratio. Also, "kink bands" in zinc due to the bending of single crystal rods have been previously reported.[19-21] These "anomalous" slip system observations that are inconsistent with the CRSS law may have been due to the boundary conditions associated with conventional axial extension or compression experiments. The 6DOF experimental technique, which allows for unconstrained motion of the crystal, shows no evidence of slip system activity other than the primary system for zinc single crystals.

To explore the possibility of cross slip and non-basal glide in Zn, a 6DOF experiment was performed on a test sample taken from an as-grown crystal that was mechanically processed by bending it slightly to introduce a small amount of cold work. The crystal was subsequently allowed to anneal at 300K for several weeks prior to test sample fabrication. Bending of Zn crystals is known to kinematically activate non-basal slip systems, for example pyramidal and prismatic planes. Also, it has been established that at room temperature (about 300K) Zn is fully annealed in a period of less than 24 hours.[3]

A 6DOF test sample from the "cold worked and annealed" Zn crystal was fabricated and tested in exactly the same manner as the previous zinc crystal. The orientation of the lattice with respect to the laboratory coordinate system and the stress strain curve is shown in Figure 11. Similar yield point and work hardening rates relative to the first experiment suggest that the crystal was fully annealed. The image correlation data shown in Figure 12 shows that slip occurred on the primary slip system, and in addition, a significant amount of slip occurred orthogonal to the basal plane. (Note that we see from inspection that the deformation on the A face was very nearly plane strain in nature, similar to the previous experiment on pristine Zn.)

The amount of primary slip system activity was determined, as described above, and is shown in Figure 13. A similar analysis (Figure 13) shows that the slip normal to the basal plane occurred proportionally during the deformation at a ratio of about 1 to 3, relative to the primary slip. Analysis of this slip activity is contained elsewhere,[22] but it is

important to point out two key points: 1) that the resolved shear stresses on the non-basal plane systems are on the order of those of the basal plane, hence the cross slip occurred at a resolved shear stress well below the known CRSS values for the non-basal slip systems; 2) since there are no slip systems orthogonal to the primary slip plane and direction, there are two possibilities to maintain the "plane strain" condition observed. The slip normal to the basal plane could either be due to a combination of non-basal slip system activities (e.g. 2nd order pyramidal systems), or through a kink band mechanism,[19-21] which involves the evolution of primary edge dislocation structures.

Since the 6DOF experiment was shown to be capable of allowing essentially unconstrained slip system activity as demonstrated by the first experiment, the observation of cross slip normal to the primary is believed to be a result of internal stress. It is possible that the processing of the zinc crystal created dislocation sources on pyramidal and/or prismatic slip systems that did not anneal out of the crystal. Under the condition of uniaxial stress loading, the applied load in combination with internal stress acted to operate the non-basal slip systems that resulted in plasticity orthogonal to the primary slip system.

VI. Summary and Conclusions

We have presented a detailed account of a new experimental technique to study crystallographic slip system activity in metallic single crystals deformed under a condition of uniaxial stress. We show that the experimental results associated with a high-quality zinc single crystal are precisely consistent with the theoretical predicted shape change (sample distortion) assuming that the most favored slip system on the basal plane is the only one that is active. This result, together with IC data allows error bars to be established for the determination of the tau-gamma (shear stress vs. shear strain) curve for the primary slip system. The following conclusions can be drawn from this work:

1) The 6DOF experiment allows unconstrained shape change in highly anisotropic materials such as Zn. Unlike previous studies on hcp crystals using conventional testing techniques which have various constraints due to boundary conditions,

there is no evidence of slip activity that is inconsistent with the CRSS law in a high-quality crystal.

2) Relatively small amounts of axial compression in highly anisotropic materials such as Zn single crystals can result in lateral displacements that have significant effects on resolved shear stresses. A FEM analysis shows that the variation in axial stress at the maximum axial strain of 0.006 was approximately $\pm$ 10%.
3) The observation of cross slip in a Zn test sample that was taken from a "cold worked and annealed" single crystal clearly show a substantial deviation from the CRSS theory.

Acknowledgements

We would like to thank Scott Perfect for performing the finite element analysis of the 6DOF experiment and deformed zinc single crystal, and Ann Bliss for performing the back-scatter Laue x-ray work to determine crystallographic orientations. This work was funded by the LLNL "Dynamics of Metals" and Laboratory Directed Research and Development programs. This work was performed under the auspices of the U.S. Department of Energy by University of California, Lawrence Livermore National Laboratory under Contract W-7405-Eng-48.

References

1. G. I. Taylor and C. F. Elam, *Proc. Roy. Soc. A*, 1923, vol. **102A**, pp. 643.

2. G. I. Taylor and C. F. Elam, *Proc. Roy. Soc. A*, 1925, vol. **108**, pp. 28.

3. E. Schmid and I. W. Boas, *Plasticity of Crystals,* Chapman and Hall LTD, London, 1950.

4. A. F. Brown, *Adv. Phys., supp. Phil. Mag.*, 1952, vol. **1**, pp. 427-479.

5. C. Barrett and T. B. Massalski, *Structure of Metals*, 3rd ed. Materials Science and Engineering, McGraw-Hill, New York, NY, 1966.

6. G. I. Taylor and W. S. Farren, *Proc. Roy. Soc. A*, 1926, vol. **111A**, pp. 529-551.

7. E. A. Avallone and T. Baumeister III,*Marks' Standard Handbook for Mechanical Engineers*, 9th ed., McGraw-Hill, New York, NY, 1987, Pages.

8. D. H. Lassila, M. M. LeBlanc and G. J. Kay, *J. Eng. Mat. & Tech.-Trans. of the ASME*, 2002, vol. **124**, pp. 290-296.

9. M. M. LeBlanc, J. N. Florando, D. H. Lassila, J. Tyson III and T. Schmidt, *Exp. Tech.*, 2006, vol. **30**, pp. 33-37.

10. P. Rosbaud and E. Schmid, *Z. Phys*, 1925, vol. **32**, pp. 197.

11. H. Mark, M. Polanyi and E. Schmid, *Z. Phys*, 1923, vol. **12**, pp. 58-116.

12. D. C. Jillson, *J. of Metals. Trans. AIME*, 1950, vol. **188**, pp. 1129-1133.

13. T. Schmidt, J. Tyson and K. Galanulis, *Exp. Tech*, 2003, vol. **27**, pp. 22-26.

14. W. H. Peters and W. F. Ranson, *Opt. Eng.*, 1982, vol. **21**, pp. 427-431.

15. A. Seeger, *Dislocations and Mechanical Properties of Crystals*, 1956, 243-325.

16. R. Parisot, S. Forest, A. F. Gourgues, A. Pineau and D. Mareuse, *Comp. Mat. Sci.*, 2000, vol. **19**, pp. 189-2004.

17. R. L. Bell and R. W. Cahn, *Roy Soc. Proc. A*, 1956, vol. **239**, pp. 494-520.

18. J. J. Fundeberger, M. J. Philippe, F. Wagner and C. Esling, *Acta Mater.*, 1997, vol. **45**, pp. 4041-4055.

19. E. Orowan, *Nature*, 1942, vol. **149**, pp. 643.

20. J. B. Hess and C. S. Barrett, *Met. Trans.*, 1949, vol. **185**, pp. 599-606.

21. J. J. Gilman and T. A. Read, *J. of Metals. Trans. AIME*, 1953, vol. **197**, pp. 49.

22. J. N. Florando, M. Rhee, A. Arsenlis, M. M. LeBlanc and D. H. Lassila, *Phil. Mag. Let.*, 2006, vol. **86**, pp. 795-805.

Figure Captions

Figure 1. Distortion of single crystals due to plastic deformation. a) Unconstrained shape change due to a uniform "uniaxial" stress state. b) non-uniform shape change during axial extension of a single crystal and accompanying lattice rotations.[5] c) Compression experiment performed using parallel platens, showing lattice rotation and frictional constraints.[5]

Figure 2. a) Schematic of the 6 Degrees of Freedom experiment. The objective is to allow unconstrained shape change. The axiality of the stress state degrades as the sample distorts, however it can be easily determined using a linear elastic 3-D finite element simulation using the elastic constants for zinc (as shown in Figure 8). b) An engineering drawing of the test sample is shown with the required dimensional tolerances.

Figure 3. A cut away scaled drawing for the 6 DOF experiment. Much of the focus on the design and construction of the experiments was on precise alignment of the half sphere over the centerline of the test sample. Using the alignment disc, the sample is positioned within 25μm of the centerline.

Figure 4. a) Crystallographic orientation of the zinc test sample and the laboratory coordinate system. b) The stereographic projection indicating the compression axis is shown. The orientation was determined using the Laue back reflection x-ray diffraction technique and has an accuracy of $\pm$0.5 degree.

Figure 5. Axial stress-strain response of the zinc single crystal. The difference between the two curves can be attributed to the extensometer measuring the displacement between the half sphere and the bottom translation platen, while the image correlation data is measuring the strain directly on the sample.

Figure 6. Axial strain in the zinc crystal derived from the image correlation technique. The final strain box also shows the axial strain map for the adjacent face. The technique is based on the determination of in-plane and out-of-plane displacement fields relative to a fixed laboratory reference frame, from which strains are calculated.

Figure 7. a) Schematic of a slip plane and direction in relation to the compression axis. b) The theoretical translation, calculated using equation 2, of the bottom of the test sample with respect to the top for a given axial compression assuming that slip only occurs on the primary slip system. The image correlation data was used to determine the translation that occurred during the experiment, and the close agreement suggests that slip occurred only on the primary slip system, in agreement with the "critical resolved shear stress" theory.

Figure 8. Elastic finite element analysis using NIKE3D to determine the maximum variation in axial stress during the experiment. The analysis was performed using the following elastic constants; c11= 161, c12= 32.4, C13 = 50.1, C33 = 61, C44 = 38.3, C66 = 63.4 (all units in GPa).a) The analysis allows the bottom to translate freely, while

loading the half sphere b) A slice taken through the center of the sample showing the variation in axial stress.

Figure 9. Image correlation technique applied to determine shear strain of the primary slip system assuming single slip on the primary slip system. A slight error is introduced due to the misalignment of the primary slip direction with the side of the sample, which is estimated to be on the order of 5%.

Figure 10. Plot of the resolved shear stress versus shear strain for the primary slip system. The shear stress is calculated by resolving the axial stress onto the primary slip plane (Schmid Factor), and IC is used to calculate the shear strains. The dash lines represent the variation in the resolved shear stress determined from the FEM analysis. The error bars in gamma are calculated from a 5mm by 5mm area in the sample where the deformation was nominally uniform.

Figure 11. a) Crystallographic orientation of the pre-bent Zn test sample. b)Axial stress-strain response for the pristine and pre-bent Zn samples. The pristine Zn has a higher flow stress because the Schmid Factor for the primary slip system is less than for the pre-bent sample. Therefore, a higher axial stress is required to achieve a similar resolved shear stress.

Figure 12. IC axial strain maps for the pre-bent Zn crystal, with the trace of the basal plane shown. The maps show activity on the basal plane as well as activity 90^{o} to the basal plane. The final strain box shows the axial strains on an adjacent face.

Figure 13. Plot showing the displacement gradient along the basal (primary) slip plane, and the displacement gradient orthogonal to the basal plane. Since there are no slip systems directly orthogonal to the primary system, it is likely that a combination of the pyramidal system must be operating to produce this strain.

Figures

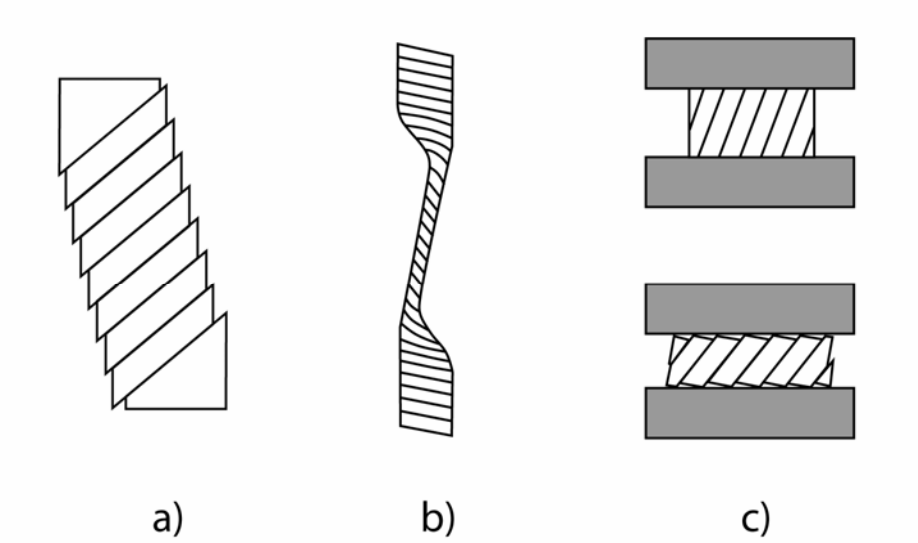

Figure 1. Distortion of single crystals due to plastic deformation. a) Unconstrained shape change due to a uniform "uniaxial" stress state. b) non-uniform shape change during axial extension of a single crystal and accompanying lattice rotations.[5] c) Compression experiment performed using parallel platens, showing lattice rotation and frictional constraints.[5]

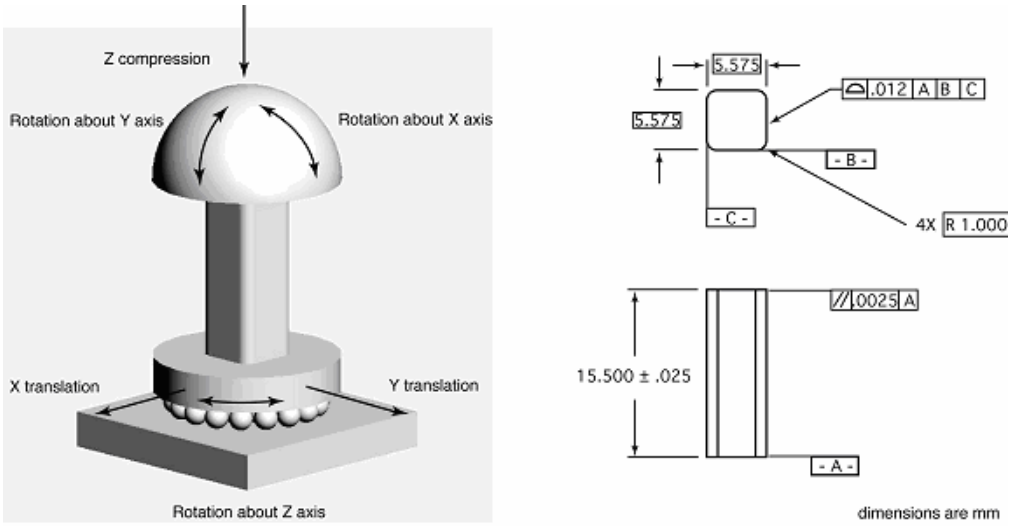

Figure 2. a) Schematic of the 6 Degrees of Freedom experiment. The objective is to allow unconstrained shape change. The axiality of the stress state degrades as the sample distorts, however it can be easily determined using a linear elastic 3-D finite element simulation using the elastic constants for zinc (as shown in Figure 8). b) An engineering drawing of the test sample is shown with the required dimensional tolerances.

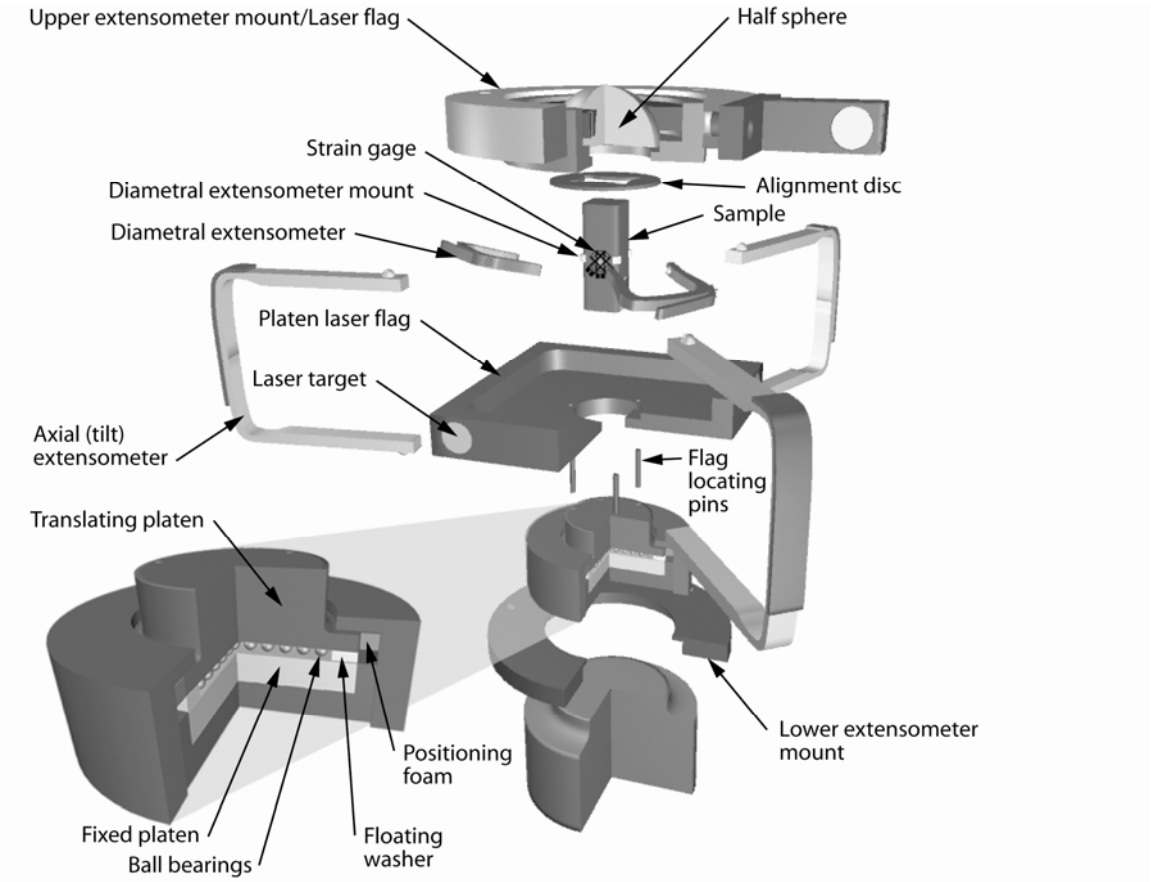

Figure 3. A cut away scaled drawing for the 6 DOF experiment. Much of the focus on the design and construction of the experiments was on precise alignment of the half sphere over the centerline of the test sample. Using the alignment disc, the sample is positioned within 25μm of the centerline.

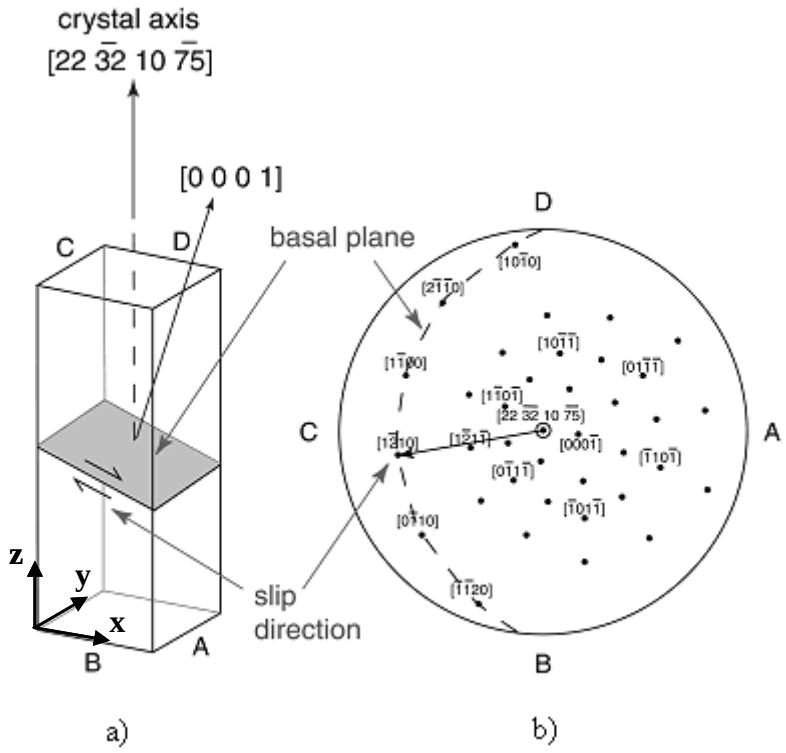

Figure 4. a) Crystallographic orientation of the zinc test sample and the laboratory coordinate system. b) The stereographic projection indicating the compression axis is shown. The orientation was determined using the Laue back reflection x-ray diffraction technique and has an accuracy of $\pm$0.5 degree.

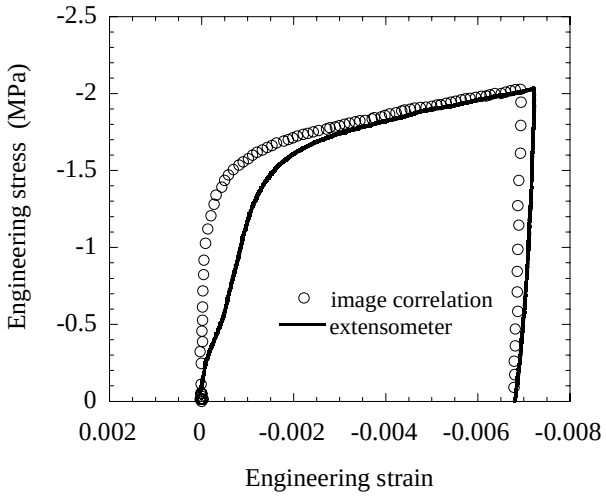

Figure 5. Axial stress-strain response of the zinc single crystal. The difference between the two curves can be attributed to the extensometer measuring the displacement between the half sphere and the bottom translation platen, while the image correlation data is measuring the strain directly on the sample.

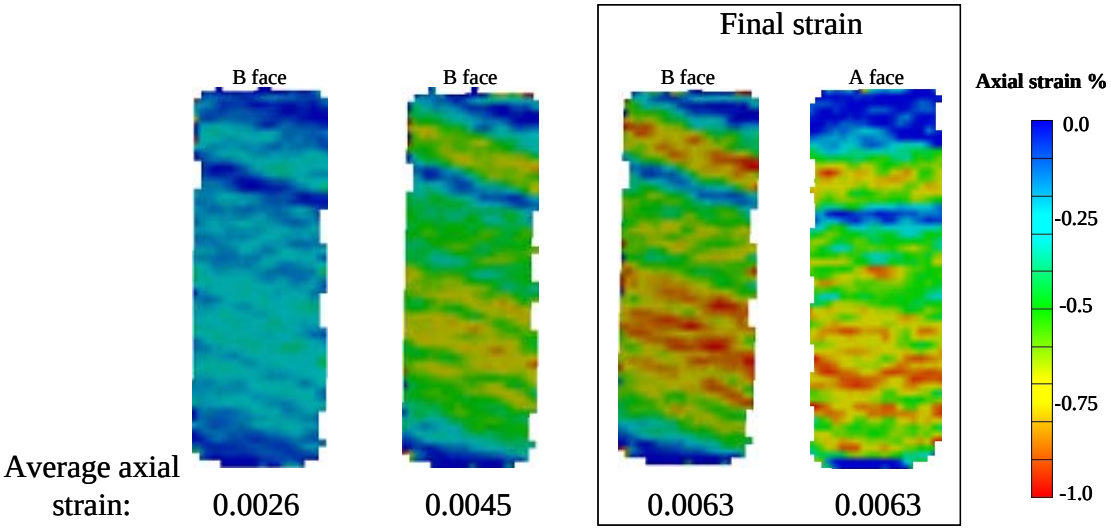

Figure 6. Axial strain in the zinc crystal derived from the image correlation technique. The final strain box also shows the axial strain map for the adjacent face. The technique is based on the determination of in-plane and out-of-plane displacement fields relative to a fixed laboratory reference frame, from which strains are calculated.

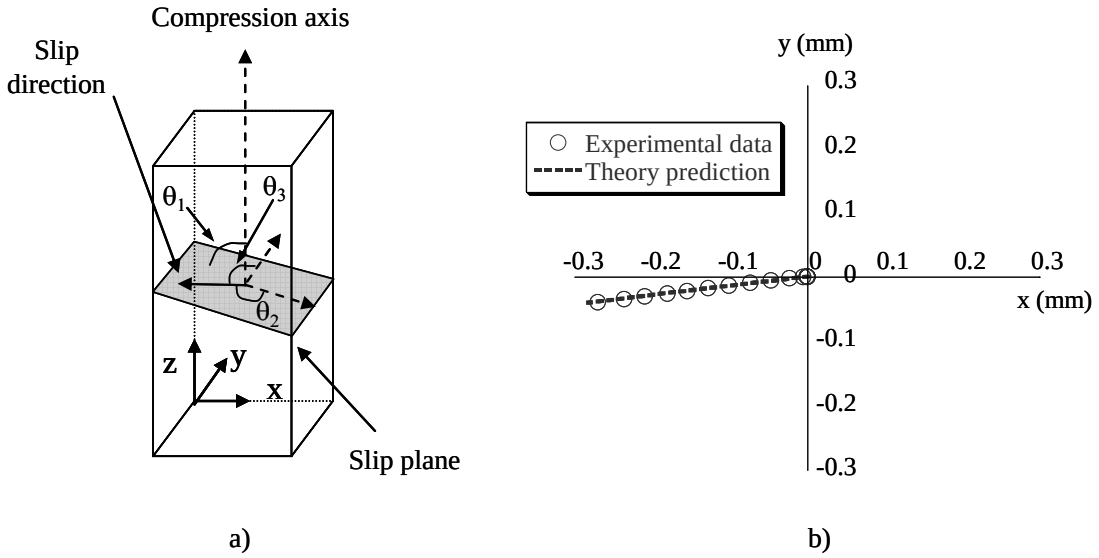

Figure 7. a) Schematic of a slip plane and direction in relation to the compression axis. b) The theoretical translation, calculated using equation 2, of the bottom of the test sample with respect to the top for a given axial compression assuming that slip only occurs on the primary slip system. The image correlation data was used to determine the translation that occurred during the experiment, and the close agreement suggests that slip occurred only on the primary slip system, in agreement with the "critical resolved shear stress" theory.

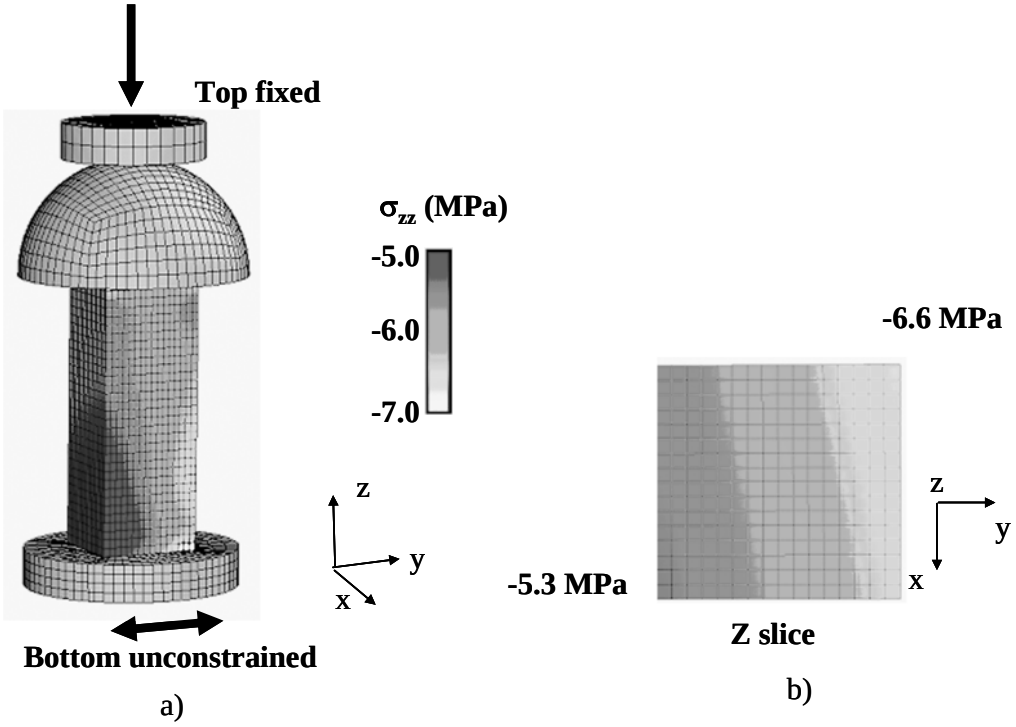

Figure 8. Elastic finite element analysis using NIKE3D to determine the maximum variation in axial stress during the experiment. The analysis was performed using the following elastic constants; c11= 161, c12= 32.4, C13 = 50.1, C33 = 61, C44 = 38.3, C66 = 63.4 (all units in GPa).a) The analysis allows the bottom to translate freely, while loading the half sphere b) A slice taken through the center of the sample showing the variation in axial stress.

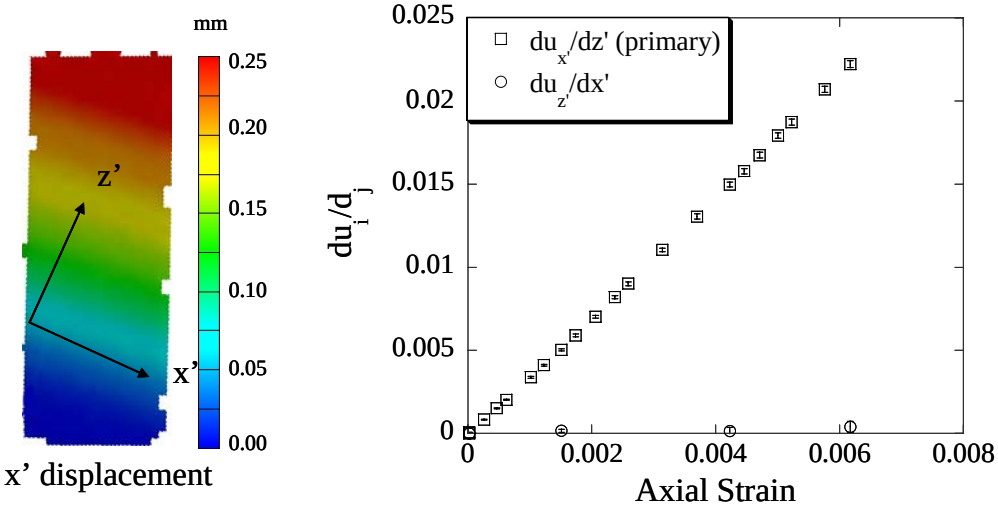

Figure 9. Image correlation technique applied to determine shear strain of the primary slip system assuming single slip on the primary slip system. A slight error is introduced due to the misalignment of the primary slip direction with the side of the sample, which is estimated to be on the order of 5%.

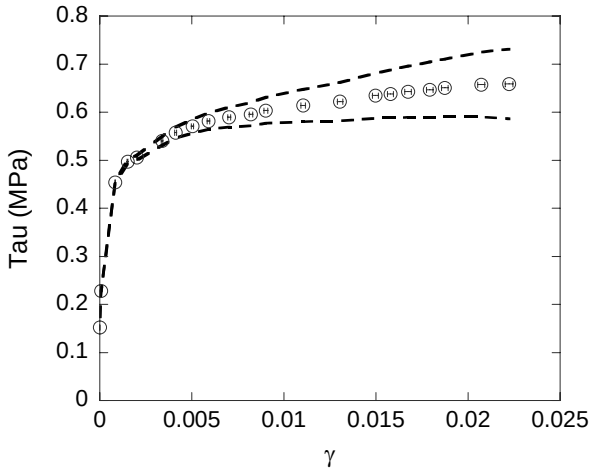

Figure 10. Plot of the resolved shear stress versus shear strain for the primary slip system. The shear stress is calculated by resolving the axial stress onto the primary slip plane (Schmid Factor), and IC is used to calculate the shear strains. The dash lines represent the variation in the resolved shear stress determined from the FEM analysis. The error bars in gamma are calculated from a 5mm by 5mm area in the sample where the deformation was nominally uniform.

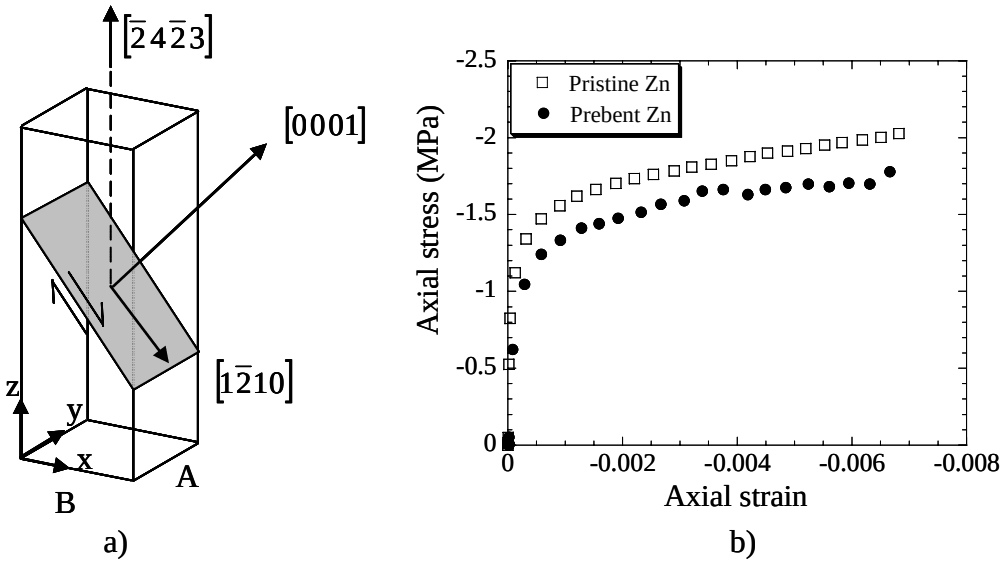

Figure 11. a) Crystallographic orientation of the pre-bent Zn test sample. b)Axial stress-strain response for the pristine and pre-bent Zn samples. The pristine Zn has a higher flow stress because the Schmid Factor for the primary slip system is less than for the pre-bent sample. Therefore, a higher axial stress is required to achieve a similar resolved shear stress.

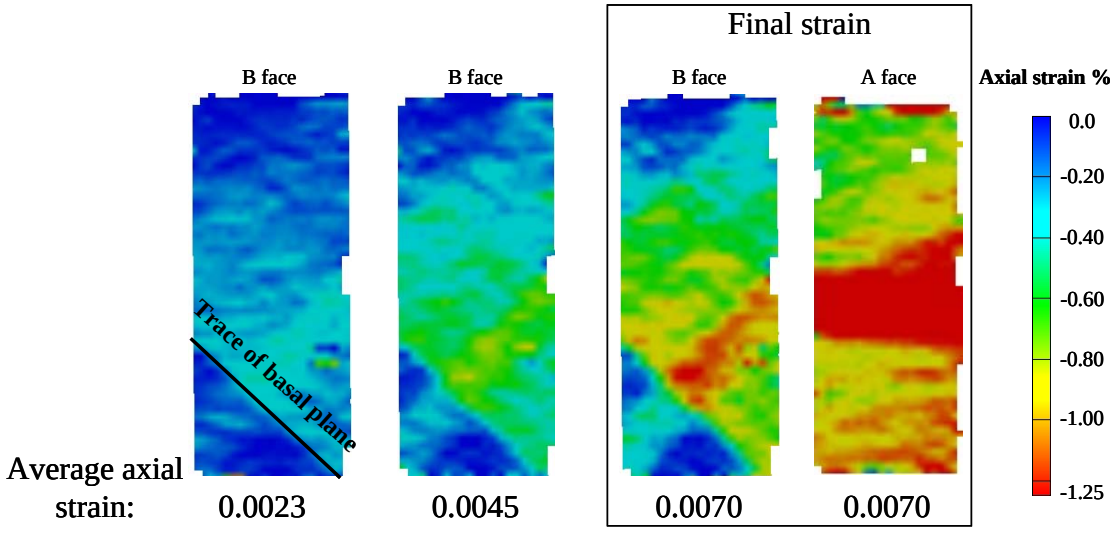

Figure 12. IC axial strain maps for the pre-bent Zn crystal, with the trace of the basal plane shown. The maps show activity on the basal plane as well as activity 90^{o} to the basal plane. The final strain box shows the axial strains on an adjacent face.

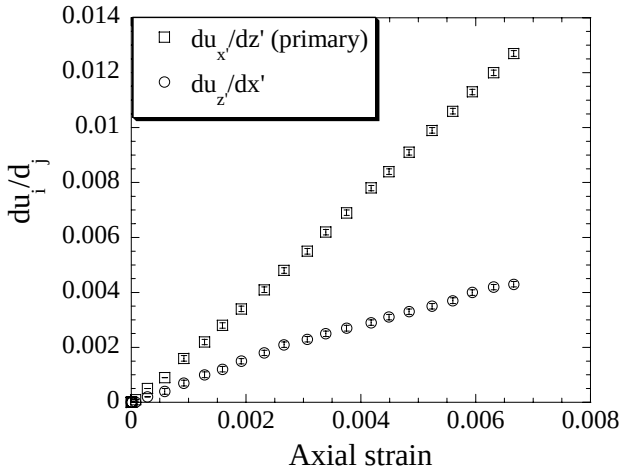

Figure 13. Plot showing the displacement gradient along the basal (primary) slip plane, and the displacement gradient orthogonal to the basal plane. Since there are no slip systems directly orthogonal to the primary system, it is likely that a combination of the pyramidal system must be operating to produce this strain.